International Journal of Thermophysics, Vol. 28, No. 4, August 2007 (© 2007)
DOI: 10.1007/s10765-007-0198-7

Reference Viscosities of H_2, CH_4, Ar, and Xe at Low Densities

Eric F. May,[1,2] Robert F. Berg,[1,3] and Michael R. Moldover[1]

Received March 26, 2007

The zero-density viscosity $\eta_{0,T}^{\text{gas}}$ of hydrogen, methane, and argon was determined in the temperature range from 200 to 400 K, with standard uncertainties of 0.084% for hydrogen and argon and 0.096% for methane. These uncertainties are dominated by the uncertainty of helium's viscosity $\eta_{0,T}^{\text{He}}$, which we estimate to be 0.080% from the difference between *ab initio* and measured values at 298.15 K. For xenon, measurements ranged between 200 and 300 K and the zero-density viscosity $\eta_{0,T}^{\text{Xe}}$ was determined with an uncertainty of 0.11%. The data imply that xenon's viscosity virial coefficient is positive over this temperature range, in contrast with the predictions of corresponding-states models. Furthermore, the xenon data are inconsistent with Curtiss' prediction that bound pairs cause an anomalous viscosity decrease at low reduced temperatures. At 298.15 K. the ratios $\eta_{0,298}^{\text{Ar}}/\eta_{0,298}^{\text{He}}$, $\eta_{0,298}^{\text{CH}_4}/\eta_{0,298}^{\text{He}}$, $\eta_{0,298}^{\text{H}_2}/\eta_{0,298}^{\text{He}}$, $\eta_{0,298}^{\text{Xe}}/\eta_{0,298}^{\text{He}}$, $\eta_{0,298}^{\text{N}_2}/\eta_{0,298}^{\text{He}}$, and $\eta_{0,298}^{\text{C}_2\text{H}_6}/\eta_{0,298}^{\text{He}}$ were determined with a relative uncertainty of less than 0.024% by measuring the flow rate of these gases through a quartz capillary while simultaneously measuring the pressures at the ends of the capillary. Between 200 and 400 K, a two-capillary viscometer was used to determine $\eta_{0,T}^{\text{gas}}/\eta_{0,T}^{\text{He}}$ with an uncertainty of 0.024% for H_2 and Ar, 0.053% for CH_4, and 0.077% for Xe. From $\eta_{0,T}^{\text{gas}}/\eta_{0,T}^{\text{He}}$, $\eta_{0,T}^{\text{gas}}$ was computed using the values of $\eta_{0,T}^{\text{He}}$ calculated *ab initio*. Finally, the thermal conductivity of Xe and Ar was computed

[1]Process Measurements Division, National Institute of Standards and Technology, Gaithersburg, Maryland 20899-8360, U.S.A.
[2]School of Oil and Gas Engineering, University of Western Australia, Crawley, WA 6009, Australia.
[3]To whom correspondence should be addressed. E-mail: robert.berg@nist.gov

from $\eta_{0,T}^{\text{gas}}$ and values of the Prandtl number that were computed from interatomic potentials. These results may help to improve correlations for the transport properties of these gases and assist efforts to develop *ab initio* two- and three-body intermolecular potentials for these gases. Reference viscosities for seven gases at 100 kPa are provided for gas metering applications.

KEY WORDS: argon; capillary viscometer; intermolecular potential; helium; hydrogen; methane; thermal conductivity; viscosity; viscosity ratio; xenon

1. INTRODUCTION

The use of *ab initio* calculations in molecular physics and chemistry is growing rapidly. Recently, we improved the technique for viscosity-ratio measurements to achieve uncertainties sufficiently small that viscosity ratios can sensitively test very accurate *ab initio* calculations [1]. Reference [1] describes the technique and results obtained for argon. This article reports new, zero-density viscosity data for methane, hydrogen, and xenon, together with slightly revised values for argon.

The motivation for the argon measurements was to improve argon-based, primary acoustic thermometry and acoustic re-determinations of the universal gas constant, both of which require accurate values of the thermal conductivity $\lambda_{0,T}^{\text{Ar}}$ of low-density argon. [2–5]. We used the viscosity data to determine $\lambda_{0,T}^{\text{Ar}}$ and $\lambda_{0,T}^{\text{Xe}}$ with smaller uncertainties than those attained by direct measurements of the thermal conductivity. (The notation uses a superscript to denote the gas; the first subscript is the pressure in kilopascals and the second subscript is the temperature in kelvin.) The motivation for the present xenon measurements was to test Curtiss' prediction [6] that bound pairs cause an anomalous decrease of the viscosity at low density and low reduced temperatures. Our xenon data are not consistent with Curtiss' prediction. At our lowest temperature of 203 K (a reduced temperature of 0.886 relative to xenon's Lennard–Jones well depth of 229 K [7]), Curtiss predicts that bound pairs reduce the viscosity by 1.15% relative to the value calculated using the pair potential of Dham et al. [8] with conventional statistical mechanics [7]. We found the ratio $\eta_{0,T}^{\text{Xe}} / \left(\eta_{0,T}^{\text{Xe}}\right)_{\text{Dham}}$ (where the numerator is our measured value) to be approximately temperature independent and, at 203 K, the measured ratio was 0.69% greater than predicted by Curtiss.

The new data for methane and hydrogen will test and possibly help to improve molecular pair potentials calculated *ab initio* by Vogel and co-workers at the University of Rostock [9]. The improved transport property correlations that result from these data will also assist industry. For

example, more accurate viscosity values for hydrogen will improve the accuracy of laminar flow elements that monitor the flow of hydrogen. We include tabulated viscosities at 100 kPa to assist with this and other gas metering applications.

We obtained the viscosity for each gas from the expression,

$$\eta_{0,T}^{\text{gas}} = \eta_{0,298}^{\text{He}} \left(\frac{\eta_{0,T}^{\text{He}}}{\eta_{0,298}^{\text{He}}} \right)_{ab\,initio} \left(\frac{\eta_{0,298}^{\text{gas}}}{\eta_{0,298}^{\text{He}}} \right) R_{T,298}^{\text{gas,He}} . \tag{1}$$

Equation (1) has four factors: (a) a reference value $\eta_{0,298}^{\text{He}}$ for the viscosity of helium at zero density and 298 K deduced from the best measurements and the best value calculated *ab initio*, (b) the temperature-dependent ratio $\left(\eta_{0,T}^{\text{He}}/\eta_{0,298}^{\text{He}}\right)_{\text{ab initio}}$ calculated *ab initio* from quantum mechanics and statistical mechanics [10,11], (c) the viscosity ratio $\eta_{0,298}^{\text{gas}}/\eta_{0,298}^{\text{He}}$ that we measured at 298.15 K, and (d) our measurements of the temperature-dependent ratio of viscosity ratios,

$$R_{T,298}^{\text{gas,He}} \equiv \left(\frac{\eta_{0,T}^{\text{gas}}}{\eta_{0,T}^{\text{He}}} \right) \Big/ \left(\frac{\eta_{0,298}^{\text{gas}}}{\eta_{0,298}^{\text{He}}} \right). \tag{2}$$

For the monatomic gases, we then obtained the thermal conductivity from

$$\lambda_{0,T}^{\text{gas}} = \frac{5R}{2} \frac{\eta_{0,T}^{\text{gas}}}{M\,\text{Pr}_{0,T}^{\text{gas}}}. \tag{3}$$

Equation (3) contains the ideal-gas molar heat capacity of a monatomic gas $C_p = 5R/2$, where R is the universal gas constant, M is the molar mass, and $Pr \equiv \eta C_p/(\lambda M)$ is the Prandtl number that we calculated from interatomic potentials. The uncertainty of $\lambda_{0,T}^{\text{gas}}$ computed from Eq. (3) is smaller than the uncertainty of direct measurements of the thermal conductivity.

We combined two approaches to measure viscosity ratios. First, we determined the reference ratio $\eta_{0,298}^{\text{gas}}/\eta_{0,298}^{\text{He}}$ by measuring the flow rate of helium and the test gas through a single quartz capillary at 298.15 K while measuring the pressures at the ends of the capillary. Then, we measured the ratio of viscosity ratios $R_{T,298}^{\text{gas,He}}$ in the temperature range $200\,\text{K} < \text{T} < 400\,\text{K}$ by using the two-capillary viscometer sketched in Fig. 1. The upstream capillary was thermostated at 298.15 K, and the downstream capillary was thermostated at test temperature T. Helium and the test gas were flowed alternately through the two-capillary viscometer while measuring the pressures at the ends of both capillaries; no flow-rate

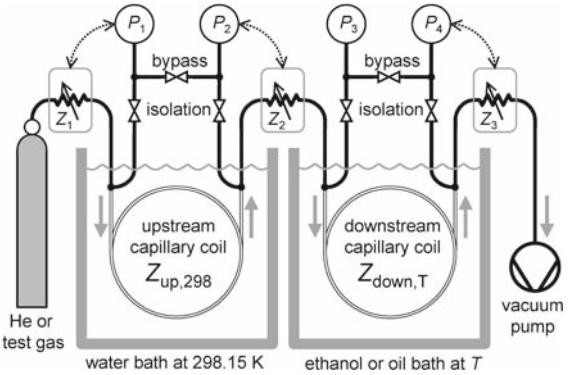

Fig. 1. Schematic diagram of the two-capillary viscometer. Impedances Z_{up} and Z_{down} were coiled nickel capillaries with a length of 7 m and an inside diameter of 0.8 mm. Variable impedances Z_1 and Z_3 were piezoelectric gas leak valves, and Z_2 was either a leak valve or a mass flow controller.

Table I. Parameters a_0, a_1, and T_* in Eq. (4), Which Describes the Measured Viscosity Ratios (The equation for Xe is valid over the temperature range from 200 to 300 K; for the other gases, the range is 200–400 K. The rms deviation of the data from the equation is less than the uncertainty of the equation. Note that the uncertainty of $\eta^{\mathrm{He}}_{0,298}$ does not contribute to the uncertainty of Eq. (4))

Parameter	H_2	CH_4	Ar	Xe
a_0	0.45002	0.60645	1.21151	1.4046
a_1	−0.04996	−0.42551	−0.82398	−0.89709
T_* (K)	76.817	137.443	123.415	228.992
Rms deviation	0.007%	0.008%	0.006%	0.053%
Uncertainty	0.024%	0.053%	0.024%	0.077%

measurements were required to determine $R^{\mathrm{gas,He}}_{T,298}$ with the two-capillary viscometer. Combining the results from the two-capillary viscometer with those from the single-capillary viscometer produced temperature-dependent viscosity ratios that can be represented by the empirical relation,

$$\eta^{\mathrm{gas}}_{0,T}/\eta^{\mathrm{He}}_{0,T} = a_0 + a_1 \exp(-T/T_*). \tag{4}$$

Table I lists the parameters a_0, a_1, and T_* for each gas, together with the equation's uncertainty and the rms deviation of the data from the equation.

Frequently, gas viscometry has used careful measurements of the viscosity of nitrogen as a standard. In contrast, we used the viscosity of

helium calculated *ab initio* as a standard. At zero density, the uncertainty claimed for the *ab initio* value [10, 11] is comparable to the uncertainty claimed for the most accurate measurements [12–15]. As one departs from ambient temperature, the uncertainty advantage of the helium standard grows because measurement uncertainties grow faster than those of the *ab initio* values [10]. In Ref. 1, we showed that the relative uncertainty of the *ab initio* ratio $\left(\eta^{\mathrm{He}}_{0,T}/\eta^{\mathrm{He}}_{0,298}\right)_{ab\,initio}$ is 0.00006 or less in the range $200\,\mathrm{K} < \mathrm{T} < 400\,\mathrm{K}$.

The recently revised *ab initio* value [11] of $\eta^{\mathrm{He}}_{0,298}$ and the most accurate measured value [15] disagree by twice their combined uncertainty. Therefore, we anchored the *ab initio* temperature-dependent ratio $\left(\eta^{\mathrm{He}}_{0,T}/\eta^{\mathrm{He}}_{0,298}\right)_{ab\,initio}$ to the reference value $\eta^{\mathrm{He}}_{0,298}=(19.833\pm0.016)\ \mu$Pa·s [1] that encompasses both values and is consistent with the oscillating-disk measurement of Kestin and Leidenfrost [12] and with the rotating cylinder measurement made by Evers et al. [13]. The uncertainty of our results for hydrogen, methane, and argon (Table II) is dominated by the uncertainty of $\eta^{\mathrm{He}}_{0,298}$. When a more accurate reference value becomes available, we will recalculate $\eta^{\mathrm{gas}}_{0,T}$ and $\lambda^{\mathrm{gas}}_{0,T}$ from the present ratio measurements with reduced uncertainties.

The remainder of this manuscript is organized as follows. Section 2 reviews the measurement principles; Section 3 describes the apparatus and the methods; and Section 4 describes the analysis of the two-capillary viscometer data. Sections 2–4 are brief because supporting details can be found in Ref. 1. In Section 5 the results for each of the four gases are presented and compared to other measurements and to various models from the literature.

2. PRINCIPLES OF THE MEASUREMENTS

2.1. Hydrodynamic Model

We use a recent hydrodynamic model [14] that relates pressures just upstream (p_1) and downstream (p_2) of a coiled capillary to the molar flow rates $\dot{n}$ of the gas through the capillary:

$$\dot{n}=\frac{\left(p_1^2-p_2^2\right)}{Z_T\eta^{\mathrm{gas}}_{0,T}RT}C^{\mathrm{gas}}\left(T,\,p_1,\,p_2\right). \tag{5}$$

Here,

$$Z_T\equiv 16L/\left(\pi r^4\right) \tag{6}$$

Table II. Contributions, Multiplied by 10^4, to the Relative Uncertainty U_r of the transport Properties of Ar and Xe and the viscosities of H_2 and CH_4

Source	H_2	CH_4	Ar	Xe	Estimator
Reference value $\eta^{He}_{0,298}$	8.0	8.0	8.0	8.0	Inconsistent *ab initio* and measured values
Ab initio ratio $\eta^{He}_{0,T}/\eta^{He}_{0,298}$	0.6	0.6	0.6	0.6	Differences among He potentials
Reference ratio $\eta^{gas}_{0,298}/\eta^{He}_{0,298}$	1.6	1.4	1.1	1.4	Scatter of data; helium slip correction
Dependence on De	1.0	1.3	1.7	4.3	Extrapolation to zero Dean number
Scatter in $R^{gas,He}_{T,298}$	0.7	0.8	0.6	5.3	Rms deviation from Eq. (4).
Viscosity virial	0.4	4.8	1.0	3.4	Inconsistent literature measurements and/or models
Prandtl number			0.4	0.4	Differences among pair potentials
Root sum of squares	8.3	9.6	8.4	11.	

is the capillary's (gas-independent) impedance at temperature T, and r and L are the bore radius and length of the capillary coil, respectively. The factor,

$$C^{gas}(T, p_1, p_2) \equiv \left(1 + \sum_{i=1}^{5} c_i^{gas}\right) f_{cent}(De, r/R_{coil}) \tag{7}$$

contains five terms c_i^{gas} that are small corrections to Poiseuille's law for the flow of an ideal gas through a straight capillary. They account for: (a) the density virial coefficients B_ρ and C_ρ and the viscosity viral coefficient B_η, (b) slip at the capillary wall, (c) the increase in the kinetic energy of the gas as it enters the capillary, (d) gas expansion along the length of the capillary, and (e) the radial temperature distribution within the gas resulting from gas expansion and viscous dissipation. The function f_{cent} accounts for the centrifugal effect due to coiling of the capillary. It depends on the geometric ratio r/R_{coil}, where R_{coil} is the radius of curvature of the

capillary coil, and the Dean number $De \equiv (r/R_{\text{coil}})^{1/2}$ Re, where $\text{Re} \equiv 2M\dot{n}/(\pi r\bar{\eta})$ is the Reynolds number; M is the molar mass, and $\bar{\eta}$ is the viscosity at an average pressure defined by Eq. (7) of Ref. 14.

2.2. Viscosity Ratios

The hydrodynamic model is used in subtly different ways to determine the two factors in Eq. (1) that were measured in this work, namely, the reference viscosity ratios $\eta_{0,298}^{\text{gas}}/\eta_{0,298}^{\text{He}}$ and the temperature-dependent relative viscosity ratios $R_{T,298}^{\text{gas,He}}$. Figure 1 shows the two-capillary viscometer that we used to measure $R_{T,298}^{\text{gas,He}}$. The upstream capillary was maintained at the reference temperature 298.15 K; its impedance is denoted $Z_{\text{up},298} \equiv 16L_{\text{up}}, 298/(\pi r_{\text{up},298}^4)$. Similarly, the impedance of the downstream capillary at the test temperature T is denoted $Z_{\text{down},T}$.

To measure $R_{T,298}^{\text{gas,He}}$, p_1 and p_2 are maintained at constant, predetermined values by controlling the impedances Z_1 and Z_2. This establishes a stable but unknown gas flow rate $\dot{n}$ that is identical through both capillaries. If both $\dot{n}$ and $Z_{\text{down},T}$ were known, Eq. (5) could be used to determine the viscosity at the temperature T from accurate measurements of p_3 and p_4. However, since $\dot{n}$ and $Z_{\text{down},T}$ are unknown, Eq. (5) is applied separately to the upstream and downstream capillaries to eliminate $\dot{n}$ and obtain an expression for the viscosity ratio $\eta_{0,T}^{\text{gas}}/\eta_{0,298}^{\text{gas}}$ in terms of p_1, p_2, p_3, and p_4. Combining that expression for the test gas with a similar expression for the helium measurements yields the working equation:

$$R_{T,298}^{\text{gas,He}} = \frac{\left(p_3^2 - p_4^2\right)^{\text{gas}}}{\left(p_1^2 - p_2^2\right)^{\text{gas}}} \frac{\left(p_1^2 - p_2^2\right)^{\text{He}}}{\left(p_3^2 - p_4^2\right)^{\text{He}}} \frac{C^{\text{gas}}(T, p_3, p_4)}{C^{\text{He}}(T, p_3, p_4)} \frac{C^{\text{He}}(298.15\ \text{K}, p_1, p_2)}{C^{\text{gas}}(298.15\ \text{K}, p_1, p_2)}. \tag{8}$$

This procedure replaces the requirement of knowing the impedance ratio $Z_{\text{up},298}/Z_{\text{down},298}$ and the thermal expansion of the downstream capillary with the viscosity ratio $\eta_{0,T}^{\text{He}}/\eta_{0,298}^{\text{He}}$, which is known from *ab initio* calculations. The dimensions of the capillaries appear only in the correction terms of Eq. (8); therefore, approximate values of the dimensions are sufficient.

We used the variable impedances Z_1 and Z_2 (Fig. 1) to maintain p_1 and p_2 at constant values that were identical for both helium and the test gas. Although this caused the two gases to flow at slightly different rates through the apparatus, this scheme had the benefit that the $(p_1^2 - p_2^2)$ terms drop out of Eq. (8). We also used the variable impedances Z_2 and

Z_3 to achieve several different values of p_2 and p_4. The data taken at several average pressures and at several flow rates were used to verify that the flow was well described by the hydrodynamic model.

We corrected for the relative zero drifts of the pressure transducers by 'taring' the transducer zeros just before and just after every flow measurement: this was achieved by closing the isolation valves between the transducers and the viscometer and opening the bypass valves connecting the transducer pairs. The apparent values of $(p_3 - p_4)$ and $(p_1 - p_2)$ in this tare state (at the average pressures of the measurement) were used to correct the pressure differences recorded when gas flowed through the capillaries.

3. APPARATUS, MATERIALS, AND PROCEDURES

3.1. Single-Capillary Measurements at 298.15 K

The ratios $\eta^{\text{gas}}_{0,298}/\eta^{\text{He}}_{0,298}$ were measured at room temperature by flowing the test gas and helium at different times through a single coiled quartz capillary and into a primary flow meter. The primary flow meter [16], which used a piston of known diameter to control the pressure in a 1 L steel bellows, measured the molar flow rate with a fractional uncertainty of 0.02%. The viscosity ratios $\eta^{\text{gas}}_{0,298}/\eta^{\text{He}}_{0,298}$ were determined from the measured flow rate and the temperature, upstream pressure, and downstream pressure of the capillary by applying Eq. (5) twice, once for the test gas and once for helium, and then taking the ratio of these two equations.

The quartz capillary had a nominal internal diameter of 0.31 mm and a length of 3.93 m; the uncertainties of these lengths introduced negligible uncertainty into the viscosity ratio. The capillary coil was constrained by a loose helix of thin wire wound around the minor diameter of the coil. The helix was an imperfect constraint: along the length of the capillary, the local radius of curvature deviated by as much as 1 mm from the average value $R_{\text{coil}} = 85.3$ mm.

The viscosities of six gases relative to helium were measured during a period of 10 weeks. To check the stability of the measurements, several sets of measurements of nitrogen, helium, and argon were interleaved between the measurements of hydrogen, methane, ethane, and xenon. Figure 2 displays the relative deviations of the capillary flow model from the flow measured by the primary flow standard. There are systematic deviations that depend on the Dean number, which implies a small error in the centrifugal correction (in Eq. (7)), perhaps due to the non-circular variations of the capillary coil.

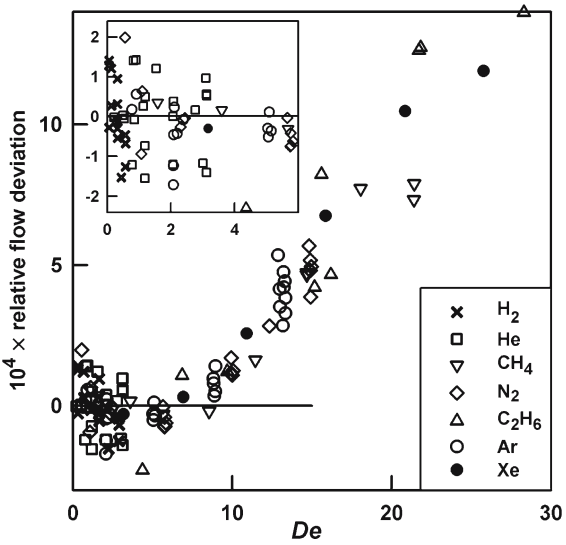

Fig. 2. Relative flow deviation defined as $\dot{n}/\dot{n}_{\text{standard}} - 1$, where $\dot{n}$ is the flow derived from the capillary-flow model and $\dot{n}_{\text{standard}}$ is the flow measured by the primary flow standard. For each gas the viscosity parameter $\eta_{0,298}^{\text{gas}}$ used when calculating $\dot{n}$ was adjusted so that the average deviation is zero for $De < 10$.

Errors due to the centrifugal correction were avoided by calculating the average viscosity using only data at $De < 10$. Table III lists the resulting viscosity ratios $\eta_{0,298}^{\text{gas}}/\eta_{0,298}^{\text{He}}$ and the associated uncertainty,

$$u\left(\eta_{0,298}^{\text{gas}}/\eta_{0,298}^{\text{He}}\right) = \left(\sigma_{\text{gas}}^2 + \sigma_{\text{He}}^2 + u_{\text{slip}}^2\right)^{1/2}. \tag{9}$$

Here, σ_{gas} is the standard deviation of the averaged data, and $u_{\text{slip}} = 0.00010$ is the uncertainty due to the uncertainty of the momentum accommodation of helium on the quartz capillary wall. The values of $\eta_{0,298}^{\text{gas}}$ listed in Table III are based on the reference value chosen for helium, whose uncertainty of 0.08% dominates the uncertainties of the values of $\eta_{0,298}^{\text{gas}}$.

The first set of hydrogen measurements was discarded because we detected pressure errors as large as 120 Pa in the readings of a 0.3 MPa full-scale gauge that was used by the primary flow standard. (We do not understand how the hydrogen caused the pressure errors because the standard contained the hydrogen in a metal bellows.) A quartz Bourdon tube gauge was used with more success. It too experienced an offset; however,

Table III. Reference Zero-Density Viscosity Ratios $\eta^{\text{gas}}_{0,298}/\eta^{\text{He}}_{0,298}$ for Seven Gases at 298.15 K Measured with the Single Quartz Capillary and a Primary Flow Meter (Zero-Density viscosities $\eta^{\text{gas}}_{0,298}$ calculated by combining the measured ratios with the reference viscosity value $\eta^{\text{He}}_{0,298} = (19.833 \pm 0.016)\mu$Pa·s [1] are also listed, as are viscosity values at 100 kPa.)

Gas	Purity (%)	$\eta^{\text{gas}}_{0,298}/\eta^{\text{He}}_{0,298}$	$\eta^{\text{gas}}_{0,298}$ (μPa·s)	$\eta^{\text{gas}}_{100,298}$ (μPa·s)
H_2	99.9999	0.44891 ± 0.00016	8.903 ± 0.016	8.904 ± 0.016
He	99.999	1.00000 ± 0.00014	19.833 ± 0.016	19.832 ± 0.016
CH_4	99.9995	0.55781 ± 0.00014	11.063 ± 0.016	11.075 ± 0.016
N_2	99.999	0.89498 ± 0.00016	17.750 ± 0.016	17.765 ± 0.016
C_2H_6	99.999	0.46562 ± 0.00024	9.235 ± 0.017	9.231 ± 0.017
Ar	99.999	1.13800 ± 0.00016	22.570 ± 0.016	22.587 ± 0.016
Xe	99.995	1.16098 ± 0.00014	23.026 ± 0.016	23.052 ± 0.016

the offset was smaller and more stable and, therefore, the resulting error could be corrected.

3.2. Two-Capillary Viscometer

The ratio of viscosity ratios $R^{\text{gas,He}}_{T,298}$ was measured in the two-capillary viscometer, which comprised two coils of electro-formed nickel tubing, each with a nominal internal diameter of 0.762 mm, a length of approximately 7.45 m, and a coil curvature radius of 0.100 m. The tubing was designed for gas chromatography, and the manufacturer claimed that it had a smooth internal surface.

The upstream reference bath was maintained at 298.15 K, with temperature fluctuations and inhomogeneities being no larger than ±2 mK. When the downstream bath was well above or below ambient temperature, the temperature fluctuations and inhomogeneities were on the order of 0.01 K. Far from ambient temperature, the uncertainty of the tabulated temperatures was approximately 0.01 K.

The manufacturer's calibration of the pressure transducers measuring p_1, p_2, and p_3 had an uncertainty of 0.008% of full scale (±12 Pa). All four pressures were measured with a resolution of 0.16 Pa. An intercomparison of the four transducers was conducted several times over the course of 6 months. A significant change was found on only one occasion: a −9 Pa shift of p_3 that was removed by taring. Furthermore, over the range of 12–150 kPa, the slopes of the four transducers remained consistent within 0.004%.

Table IV. Gas Purity (by Volume), Temperature, and Flow Ranges and Corresponding Dean Numbers for Measurements with the Two-Capillary Viscometer (Not all flow rates were used at all temperatures. The maximum Dean number occurred at the minimum temperature.)

Gas	Purity	Temperature range (K)	Flow rate (μmol·s^{-1})	*De* (at 298 K)	*De* (maximum)
H_2	99.9999%	213.62–394.21	39–81	0.9–1.9	2.3
He	99.9999% (< 0.2 ppm H_2O)	202.71–394.21	7.8–72	0.2–1.5	2.0
CH_4	99.9995% (< 1.8 ppm H_2O)	210.76–391.55	31–65	4.7–9.7	10.7
Ar	99.9995%	202.71–394.20	26–73	4.9–11.6	16.4
Xe	99.999%	202.88–298.15	4.5–25	2.7–14.6	21.9

The pressures p_1, p_2, and p_4 were controlled at their set points using the variable impedances Z_1, Z_2, and Z_3 and digital PID algorithms. At each flow rate, p_4 was controlled sequentially at six different set points within the range from 13 to 75 kPa. For the argon measurements, the set-point for p_1 was fixed at 140 kPa while p_2 was stepped through the values of 115, 120, 125, and 130 kPa. For the other gases, p_1 and p_2 were varied slightly to accommodate their differing viscosities. Typically, p_1 was fixed at approximately 115 kPa, and the four values of p_2 ranged from 100 to 108 kPa. Table IV gives the resulting flow ranges and the gas purities claimed by the gas suppliers. The uncertainty contributed by the gas impurity was an order of magnitude smaller than other uncertainties.

4. ANALYSIS

4.1. Data Reduction

For a given flow condition, the steady-state pressures were converted to difference pressures ($\Delta p_{34} \equiv p_3 - p_4$, $\Delta p_{12} \equiv p_1 - p_2$) and mean pressures [$\bar{p}_{12} \equiv (p_1 + p_2)/2$, $\bar{p}_{34} \equiv (p_3 + p_4)/2$]. The difference pressures were corrected by a tare value, and then the nominal capillary dimensions were used to calculate the ratio,

$$\Xi^{\text{gas}}(T) \equiv \frac{\Delta p_{34}\bar{p}_{34}}{\Delta p_{12}\bar{p}_{12}} \frac{C^{\text{gas}}(T, p_3, p_4)}{C^{\text{gas}}(298\ \text{K}, p_1, p_2)} = \frac{Z_{\text{down},T}}{Z_{\text{up},298}} \frac{\eta^{\text{gas}}_{0,T}}{\eta^{\text{gas}}_{0,298}} \frac{T}{298.15\ \text{K}}. \quad (10)$$

For a given flow rate, adjusting all the values of $\bar{p}_{34}$ by +9 Pa decreased the scatter of the six values of $\Xi^{\text{gas}}(T)$ corresponding to the six different exit pressures. Since this adjustment was within the pressure uncertainty, it

was applied to all the data reported here. (Adjusting $\bar{p}_{12}$ within its uncertainty did not have a similar effect.)

The values of $\Xi^{\text{gas}}(T)$ depended on the Dean number of the fluid in the downstream capillary. This dependence decreased with the Dean number, and the values of $\Xi^{\text{He}}(298\,\text{K})$ were virtually independent of De. Therefore, we determined $R_{T,298}^{\text{gas,He}}$ from $\Xi^{\text{gas}}(T)$ and $\Xi^{\text{He}}(T)$ using the equation,

$$R_{T,298}^{\text{gas,He}} = \lim_{De\to 0} \Xi^{\text{gas}}(T) / \lim_{De\to 0} \Xi^{\text{He}}(T). \tag{11}$$

Further details about the extrapolation to zero Dean number are given in Section 4.2.

When the temperature of both capillaries was 298.15 K, Eq. (10) reduced to $\Xi^{\text{gas}}(298\,\text{K}) = Z_{\text{down},298}/Z_{\text{up},298}$, allowing a determination of the (gas-independent) impedance ratio of the capillaries from pressure measurements. The impedance ratio $Z_{\text{down},298}/Z_{\text{up},298}$ was determined on several occasions over an 8-month period and usually decreased with time. This might have been caused by a gradual decrease of r_{up} resulting from the accumulation of particles or of an oil film in this capillary. (The gas from the supply cylinders always passed through particulate filters before entering the capillaries.) However, the drift in $Z_{\text{down},298}/Z_{\text{up},298}$ did not affect the measurements of $R_{T,298}^{\text{gas,He}}$ because we operated the two-capillary viscometer in helium-standard mode [1] (i.e., used Eq. (8), or equivalently Eq. (11)), which does not require accurate values of the impedance ratio.

4.2. Capillary Ellipticity and Extrapolation to $De = 0$

The dependence of $\Xi^{\text{gas}}(T)$ on the Dean number in the downstream capillary fell into one of two regimes. When the Dean number was less than 11, a weak linear dependence was observed. This linear dependence was sufficiently weak that extrapolating $\Xi^{\text{gas}}(T)$ to $De = 0$ did not increase the uncertainty of $R_{T,298}^{\text{gas,He}}$. For example, $\left(d \ln\left(\Xi^{\text{Ar}}(330\,\text{K})\right)/dDe\right) \cong 2 \times 10^{-5}$ and, thus, the values of $\Xi^{\text{Ar}}(330K)$ at $De = 0$ and $De = 10$ differed by 0.02% or less.

However, for $De > 11$ the dependence of $\Xi^{\text{gas}}(T)$ on De deviated from the dependence built into the hydrodynamic model [14]. One possible explanation is that the bores of the capillaries were slightly elliptical; the hydrodynamic model extends to Dean numbers well in excess of 11 *if* the capillary bore is sufficiently circular and uniform [14]. The centrifugal correction in Eq. (7) for an elliptical bore deviates from the correction for a circular bore by an amount proportional to De^4 [1], and as shown in

Fig. 5 of Ref. 1, our values of $\Xi^{Ar}(T)$ and $\Xi^{Xe}(T)$ for $De > 11$ were consistent with this De^4 model.

We therefore evaluated $\lim_{De\to 0} \Xi^{\text{gas}}(T)$ in two ways. First, the $\Xi^{\text{gas}}(T)$ data with $De < 11$ were extrapolated using a linear function of De. Second, all the $\Xi^{\text{gas}}(T)$ data were extrapolated to $De = 0$ by fitting A and B in the function $A + B\ De^4$. The difference in the two extrapolated values of $R_{T,298}^{\text{gas,He}}$ was taken to be the uncertainty resulting from the extrapolation to $De = 0$.

For helium, hydrogen, and methane, the maximum Dean number was always less than 11 (Table IV) and thus the linear function was fit to all the $\Xi^{\text{gas}}(T)$ data measured at that temperature. This was also the case for argon at temperatures above 298 K. The hydrogen and methane values reported here were obtained with the linear function.

At temperatures of 298 K or below, the $\Xi^{\text{Ar}}(T)$ and $\Xi^{\text{Xe}}(T)$ data contained values measured at $De > 11$ that were excluded from the linear extrapolation but included in the quartic extrapolation. The argon values reported here were obtained with the linear function (data with $De > 11$ were excluded). Similarly, at all but one temperature, the xenon values were obtained with the linear function. (The xenon data at 203 K had a minimum Dean number of 11.06.)

4.3. Parameters for the Hydrodynamic Model

Evaluation of the correction terms c_i^{gas} in the hydrodynamic model required up to seven parameters for each fluid: the molar mass M, the zero-density viscosity $\eta_{0,T}^{\text{gas}}$, the density virial coefficients B_ρ and C_ρ, the thermal conductivity λ, the temperature derivative of the zero-density viscosity $d\eta_{0,T}^{\text{gas}}/dT$, and the viscosity virial coefficient $B_\eta \equiv \lim_{\rho\to 0}(\partial\eta/\partial\rho)_T$. For helium, hydrogen, and argon we ignored the third density virial coefficient because the densities in this work were so low. For helium and argon, we calculated the parameters $\eta_{0,T}^{\text{gas}}$, B_ρ, λ, and $d\eta_{0,T}^{\text{gas}}/dT$ from pair potentials [11,17]. For xenon, we used the pair potential of Dham et al. [8] but took B_ρ and C_ρ from the virial equation of state of Hurly et al. [18]. For methane, we used the viscosity correlation of Vogel et al. [19] to calculate $\eta_{0,T}^{\text{gas}}$ and $d\eta_{0,T}^{\text{gas}}/dT$, while B_ρ, C_ρ, and λ were taken from the NIST Standard Reference Database 23 (REFPROP) Version 7.0 [20]. For hydrogen, $\eta_{0,T}^{\text{gas}}$, $d\eta_{0,T}^{\text{gas}}/dT$, and λ were calculated using the correlation of Assael et al. [21] and B_ρ was taken from NIST-23. We confirmed that the uncertainty of each of these parameters made a negligible contribution to the uncertainty of the measured viscosity ratios.

The viscosity virial coefficient B_η makes a significant contribution to the uncertainty budget (Table I); therefore, we consider it in some detail. The average capillary pressures spanned a very limited range (typically 43–76 kPa), so our results could not determine B_η precisely for any of the gases. For hydrogen, methane, and argon, we used values deduced from published data. Since viscosity measurements are often reported as a function of pressure, we discuss the related quantity $b_T^{\text{gas}} \equiv \lim_{p\to 0} (\partial\eta/\partial p)_T / \eta = B_\eta (\partial\rho/\partial p)_T / \eta$.

Values of b_T^{gas} can be derived either from measurements or from corresponding-states models of the type developed by Rainwater and Friend [22]. Wherever possible we used measured values because the differences between b_T^{gas} values derived from different versions of the corresponding-states models were significantly larger than the differences among measured values. For example, the relative standard deviations of b_T^{Ar} derived from Refs. 13, 23, 24, and 25, all of which are based on experimental data, are 7, 3, and 8% at 203, 298, and 392 K, respectively. In contrast, the values of b_T^{Ar} derived from the model of Rainwater and Friend [22] and its most recent modification by Vogel et al. [26] differ by 52, 26, and 20% at the same temperatures. However, for methane and xenon, corresponding-states models were used to guide the values of b_T^{gas} selected because of the insufficiency and/or inconsistency of available measured values.

For argon, we calculated b_T^{Ar} from the correlation of Lemmon and Jacobsen [23], which takes into account a wide range of measurements. We estimated its uncertainty from the inconsistencies among measurements at similar temperatures. At our lowest temperature (203 K), where the viscosity ratio is most sensitive to b_T^{Ar}, the values of b_{203}^{Ar} derived from Refs. 13 and 23–25 lie in the range (14.2 to 16.6) $\times 10^{-9}$ Pa^{-1}. The corresponding fractional uncertainty of $\eta_{0,T}^{\text{Ar}}/\eta_{0,T}^{\text{He}}$ at 203 K is 0.00010; it is smaller at higher temperatures.

For helium, b_T^{He} is more than an order of magnitude smaller than b_T^{Ar} between 200 and 400 K; its effect on the viscosity ratio is correspondingly smaller. We used the data of Gracki et al. [24] to estimate b_T^{He} at all temperatures; the corresponding uncertainty of $\eta_{0,T}^{\text{gas}}/\eta_{0,T}^{\text{He}}$ is negligible.

For hydrogen, the value of $b_T^{\text{H}_2}$ also is significantly smaller than b_T^{Ar}, and it contributed negligible uncertainty to the viscosity ratios $\eta_{0,T}^{\text{H}_2}/\eta_{0,T}^{\text{He}}$. We derived values of $b_T^{\text{H}_2}$ from the wide-ranging data of Flynn et al. [23, 30].

For methane, the discrepancies between measured values of $b_T^{\text{CH}_4}$ are similar to those of the corresponding-states models. For example, at 293 K the high-pressure viscosity measurements of Hurly et al. [27], Kestin and

Yata [28], Schley et al. [29], and Evers et al. [13] lead to $b_{293}^{CH_4}$ values in the range (8.9 to 11.9) $\times 10^{-9}$ Pa^{-1}; the models [22,26] predict values ranging from (8.5 to 12.6) $\times 10^{-9}$ Pa^{-1}. For CH_4 below 260 K, the only high-pressure viscosity measurements of reasonable precision are those of Evers et al. [13], which extend to 233 K, and those of Barua et al. [30], which extend to 223 K. The range of $b_{233}^{CH_4}$ values derived from those references is (6.2 to 19.4) $\times 10^{-9}$ Pa^{-1}, whereas the models [22,26] predict values ranging from (6.6 to 14.7) $\times 10^{-9}$ Pa^{-1}.

Thus, we took $b_T^{CH_4}$ from four sources: the data of Schley et al. [29] and Evers et al. [13], and from the two models [22,26]. At 298 K, the variation in $R_{298,298}^{CH_4,He}$ due to the range of the four values $b_{298}^{CH_4}$ was 0.00029. At temperatures below 298 K, the variation in $R_{T,298}^{CH_4,He}$ due to the source of $b_T^{CH_4}$ was 0.00026 or less, but at higher temperatures, the variation in $R_{T,298}^{CH_4,He}$ increased to a maximum of 0.00048 at 392 K. The contribution to the uncertainty of $\eta_{0,T}^{CH_4}/\eta_{0,T}^{He}$ from $b_T^{CH_4}$ is therefore estimated to be 0.00048. The values of $\eta_{0,T}^{CH_4}/\eta_{0,T}^{He}$ reported here are those calculated using the $b_T^{CH_4}$ derived from the data of Schley et al. [29] because they were most consistent with the values of $b_T^{CH_4}$ inferred from our methane data (see Section 4.4).

The analysis of the xenon data is discussed in Section 4.4 below because it is significantly different from that of the other gases. For the single quartz capillary measurements (Table III) of ethane and nitrogen, we took $b_{298}^{C_2H_6}$ from Hendl and Vogel [31] and $b_{298}^{N_2}$ from Gracki et al. [24].

In addition to the fluid parameters described above, the hydrodynamic model contains three constants that are fixed by theory (K_{ent}, K_{exp}, K_{therm}) and one constant (K_{slip}) that describes the degree of momentum accommodation at the capillary wall [14]. Our data for helium in the quartz capillary are consistent (independent of pressure) with the value $K_{slip} = 1.18$, which is similar to the values found previously [14]. For the other gases in the quartz capillary and for all gases in the nickel capillary, our results are consistent with $K_{slip} = 1.00$, which corresponds to complete momentum accommodation. For the two-capillary viscometer, we set $K_{ent} = 0$ because the matching bores of the T-unions and capillaries suppressed the kinetic energy change of gas entering the impedances. The values of K_{exp} and K_{therm} were the same as those used by Berg [14].

Four of the correction terms c_i^{gas} required an estimate of the Reynolds number. The initial values for these corrections were based on an estimate of $\dot{n}_0$, the molar flow rate obtained without applying

corrections to Poiseuille's law for a compressible fluid. Obtaining the final values required only three iterations of the model.

4.4. Analysis of the Xenon Data

For xenon, the (p, η) data of Kestin and Leidenfrost at 298 K [12] lead to a value of $b_{298}^{\mathrm{Xe}} = 11.2 \times 10^{-9}\,\mathrm{Pa}^{-1}$. The corresponding-states model of Najafi et al. [32] (which used the more accurate potential of Dham et al. [8] instead of a Lennard–Jones potential) predicts $b_{298}^{\mathrm{Xe}} = 10.2 \times 10^{-9}\,\mathrm{Pa}^{-1}$. This value is closer to the measured value than the other corresponding-states models: the Rainwater and Friend [22] model gives $b_{298}^{\mathrm{Xe}} = 8.9 \times 10^{-9}\,\mathrm{Pa}^{-1}$ while the model of Vogel et al. [26] gives $b_{298}^{\mathrm{Xe}} = -2.5 \times 10^{-9}\,\mathrm{Pa}^{-1}$. Figure 3 compares the results of using the measured value of b_{298}^{Xe} with using the modeled value from Ref. 26. For a fixed value of De, the spread in $\Xi^{\mathrm{Xe}}(298\,\mathrm{K})$ is less than 0.013% for the measured b_{298}^{Xe} but is 0.041% for the b_{298}^{Xe} from the corresponding-states model.

At reduced temperatures below 1.3, the corresponding-states models have large slopes and, consequently, they predict that b_T^{Xe} decreases rapidly below 298 K. The corresponding-states models predict b_{203}^{Xe} values in the range $(-77.6$ to $-42.9) \times 10^{-9}\,\mathrm{Pa}^{-1}$. The most positive of these is from Najafi et al. [32] and, at constant De, the resulting spread in $\Xi^{\mathrm{Xe}}(203\,\mathrm{K})$ is 0.12%. This spread increases as b_{203}^{Xe} becomes more negative. We therefore ignored the corresponding-states models and used spreads in the $\Xi^{Xe}(T)$ values to estimate $\left(b_T^{\mathrm{Xe}} - b_{298}^{\mathrm{Xe}}\right)$ from measured data.

The limited pressure range of the data precludes precise determinations of b_T^{gas}. However, from Eq. (10) it follows that $\Xi^{\mathrm{gas}}(T)$ depends upon the difference $\left(b_T^{\mathrm{gas}} - b_{298}^{\mathrm{gas}}\right)$, and if this difference is sufficiently in error, $\Xi^{\mathrm{gas}}(T)$ values measured at constant De but different pressures exhibit a large spread. We tested this method with argon and methane over the temperature range from 200 to 400 K by fixing the values of b_{298}^{gas}, allowing b_T^{gas} to vary and minimizing the spread in $\Xi^{\mathrm{gas}}(T)$ values. At all temperatures, the values of b_T^{gas} determined in this way were within $2.7 \times 10^{-9}\,\mathrm{Pa}^{-1}$ of the values taken from the literature for argon [23] and methane [29].

Thus, for xenon we used the experimental value $b_{298}^{\mathrm{Xe}} = 11.2 \times 10^{-9}\,\mathrm{Pa}^{-1}$ from Ref. 12 and obtained b_T^{Xe} values by minimizing the spread in the $\Xi^{\mathrm{Xe}}(T)$ data. The smallest of these was $b_{203}^{\mathrm{Xe}} = (0 \pm 5.2) \times 10^{-9}\,\mathrm{Pa}^{-1}$; the uncertainty estimate is based on the results of the Ar and CH_4 tests, and the fact that $\left(b_T^{\mathrm{Xe}} - b_{298}^{\mathrm{Xe}}\right)$ in the hydrodynamic model is correlated with other correction terms, such as centrifugal effects. The values of b_T^{Xe}

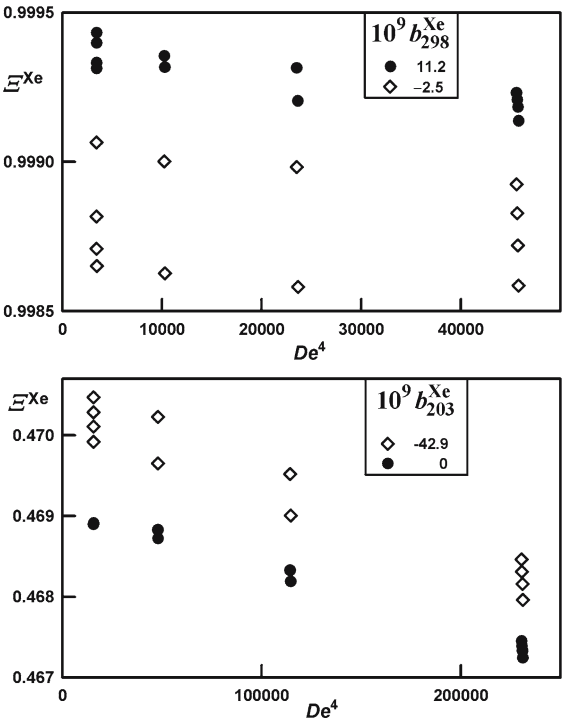

Fig. 3. Values of $\Xi^{Xe}(T)$ calculated from the present data using Eq. (10). The spread of these data places bounds on the value of b_T^{Xe}. Top: Spread due to the experimental value of b_{298}^{Xe} from Kestin and Leidenfrost [12] is less than half that due to the corresponding-states value of Vogel et al. [18]. Bottom: Optimized value of b_{203}^{Xe} produces a spread that is much less than the spread due to the corresponding-states value from Najafi et al. [32]. Note the change in scale between the top and bottom panels.

reported here and used to determine $\eta_{0,T}^{Xe}/\eta_{0,T}^{He}$ were obtained by linearly interpolating between the values of b_{203}^{Xe} and b_{298}^{Xe}. The interpolated values were preferred because they decrease monotonically with temperature and are also consistent, within the estimated uncertainty, with the b_T^{Xe} determined by minimizing the spread in the $\Xi^{Xe}(T)$ data.

The resulting values of b_T^{Xe}, listed in Table V, differ significantly from the corresponding-states values. If our xenon data were analyzed instead with values of b_T^{Xe} taken from Najafi et al. [32], the viscosity ratios $\eta_{0,T}^{Xe}/\eta_{0,T}^{He}$ would increase by up to 0.25%.

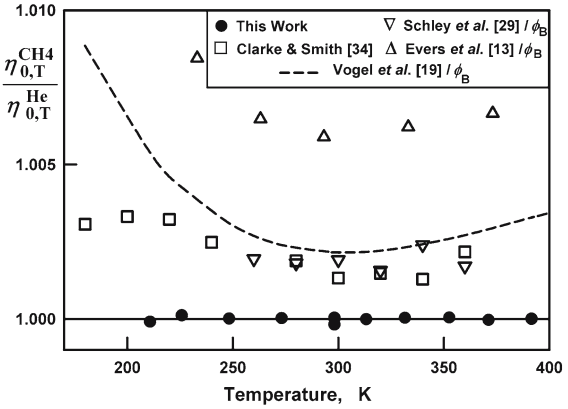

Fig. 4. Comparison of the ratio $\eta^{CH_4}_{0,T}/\eta^{He}_{0,T}$ measured in this work with the ratio measured by Clarke and Smith [34] and with ratios calculated using $\eta^{CH_4}_{0,T}$ from Refs. 13, 19, and 29 and $\eta^{He}_{0,T}$ calculated from the potential φ_B [11]. The baseline is Eq. (4) with the CH_4 parameters in Table I.

Table V. Transport Properties of Xenon at Zero Density, Together with the Values of the Viscosity Virial Coefficient b_T^{Xe} of Xenon Estimated in this Work and Reference Viscosities at 100 kPa

T (K)	$\eta^{Xe}_{0,T}/\eta^{He}_{0,T}$ ±0.077%	$\eta^{Xe}_{0,T}$ (μPa·s) ±0.11%	$\lambda^{Xe}_{0,T}$ (mW·m^{-1}·K^{-1}) ±0.11%	b_T^{Xe} (10^{-9}Pa^{-1}) $\pm 5.2\times10^{-9}$Pa^{-1}	$\eta^{Xe}_{100,T}$ (μPa·s) ±0.11%
202.882	1.03547	15.823	3.7598	0	15.823
213.014	1.05060	16.589	3.9418	1.2	16.591
227.454	1.07198	17.692	4.2038	2.9	17.697
246.053	1.09768	19.105	4.5394	5.1	19.115
275.557	1.13505	21.334	5.0691	8.6	21.352
298.147	1.16103	23.027	5.4713	11.2	23.053
298.149	1.16085	23.023	5.4705	11.2	23.049

5. RESULTS

In Ref. 1, a 0.05% error was made when calculating the values of $\eta^{Ar}_{0,T}$ and $\lambda^{Ar}_{0,T}$ because the value of $\eta^{He}_{0,298}$ used in Eq. (1) was inadvertently taken to be the value measured by Berg [14, 15], rather than the stated reference value of $(19.833 \pm 0.016)\,\mu$Pa·s. In addition, the ratios $\eta^{Ar}_{0,T}/\eta^{He}_{0,T}$ in Ref. 1 were all derived using a quartic extrapolation to $De = 0$, which

Table VI. Transport Properties of Argon at Zero Density, plus Reference Viscosities at 100 kPa

T (K)	$\eta_{0,T}^{Ar}/\eta_{0,T}^{He}$ ±0.024%	$\eta_{0,T}^{Ar}$ (μPa·s) ±0.084%	$\eta_{100,T}^{Ar}$ (μPa·s) ±0.084%	$\lambda_{0,T}^{Ar}$ (mW·m^{-1}·K^{-1}) ±0.084%
202.71	1.05206	16.067	16.092	12.550
210.75	1.06202	16.649	16.673	13.005
213.19	1.06512	16.828	16.851	13.145
223.66	1.07700	17.574	17.596	13.729
230.29	1.08403	18.041	18.063	14.094
248.14	1.10114	19.275	19.296	15.060
248.25	1.10127	19.283	19.304	15.066
273.15	1.12144	20.953	20.971	16.374
298.14	1.13791	22.568	22.585	17.639
298.14	1.13779	22.566	22.582	17.637
298.15	1.13800	22.570	22.587	17.641
298.15	1.13798	22.570	22.586	17.640
298.15	1.13792	22.568	22.585	17.639
315.33	1.14746	23.646	23.662	18.484
330.48	1.15489	24.576	24.591	19.213
335.96	1.15744	24.910	24.925	19.475
351.08	1.16351	25.810	25.823	20.181
371.45	1.17085	27.001	27.014	21.115
391.56	1.17695	28.148	28.160	22.015
391.57	1.17700	28.149	28.161	22.016
394.20	1.17779	28.299	28.311	22.133

corresponds to an error of less than 0.017%. The corrected values of $\eta_{0,T}^{Ar}/\eta_{0,T}^{He}$, $\eta_{0,T}^{Ar}$, $\eta_{100,T}^{Ar}$, and $\lambda_{0,T}^{Ar}$ are listed in Table VI.

Figure 4 compares our measurements of the viscosity ratio $\eta_{0,T}^{CH_4}/\eta_{0,T}^{He}$ with other measurements of the ratio and with calculations of that ratio from various sources of $\eta_{0,T}^{CH_4}$. The baseline of Fig. 3 is Eq. (4) with the CH_4 parameters listed in Table I; the equation fits our data with an rms deviation of 0.008%. The uncertainty of our ratio data is 0.053%. The ratios $\eta_{0,T}^{CH_4}/\eta_{0,T}^{He}$ and viscosities $\eta_{0,T}^{CH_4}$ and $\eta_{100,T}^{CH_4}$ determined in this work are listed in Table VII.

In 1968 and 1969, Clarke and Smith [33,34] published two remarkable papers that included tabulated measurements of $\eta_{0,T}^{Ar}/\eta_{0,T}^{N_2}$, $\eta_{0,T}^{He}/\eta_{0,T}^{N_2}$, $\eta_{0,T}^{CH_4}/\eta_{0,T}^{N_2}$, and $\eta_{0,T}^{Xe}/\eta_{0,T}^{N_2}$ (as well as ratios for other gases). Figure 4 shows that their data deviate from ours by a maximum of 0.33% and, on average, are only 0.21% larger. (Clarke and Smith's ratio at 260 K is not shown due to an apparent typographical error for helium in Table II of Ref. 34.) The curve in Fig. 4 was calculated by dividing values

Table VII. Viscosity of Methane at Zero Density and 100 kPa

T (K)	$\eta_{0,T}^{CH_4}/\eta_{0,T}^{He}$ ±0.053%	$\eta_{0,T}^{CH_4}$ (μPa·s) ±0.096%	$\eta_{100,T}^{CH_4}$ (μPa·s) ±0.096%
210.756	0.51458	8.067	8.080
225.810	0.52421	8.609	8.622
248.251	0.53655	9.395	9.408
273.157	0.54815	10.242	10.254
298.145	0.55785	11.064	11.075
298.149	0.55773	11.061	11.073
298.151	0.55784	11.064	11.075
313.223	0.56287	11.546	11.557
331.550	0.56834	12.121	12.132
352.568	0.57375	12.764	12.775
371.193	0.57785	13.319	13.329
391.543	0.58181	13.914	13.923
391.551	0.58181	13.914	13.923

of $\eta_{0,T}^{CH_4}$ calculated from the reference methane correlation of Vogel et al. [19] by values of $\eta_{0,T}^{He}$ calculated from the potential φ_B [11]. Our data are consistent with the calculated ratio within the uncertainty of the methane correlation, which is ±0.3% between 260 and 360 K, and ±1% at other temperatures [19].

The methane viscosity correlation of Vogel et al. [19] is based partly on data published by Schley et al. [29] who used a vibrating wire to determine $\eta_{p,T}^{CH_4}$ between 260 and 360 K at pressures to 29 MPa with a claimed uncertainty of 0.3%. Schley et al. report zero-density viscosities extrapolated from each of their isotherms, and these $\eta_{0,T}^{CH_4}$ were converted to viscosity ratios $\eta_{0,T}^{CH_4}/\eta_{0,T}^{He}$ using $\eta_{0,T}^{He}$ calculated from the potential φ_B [11]. Figure 4 shows that these data deviate from our ratios by less than 0.25%. However, the low-density data of Evers et al. [13], who used an oscillating cylinder to determine $\eta_{p,T}^{CH_4}$ with a claimed uncertainty of 0.15% in the dilute gas region, deviate from the data of Schley et al. and Clarke and Smith by 0.4%, and from our data by 0.53–0.85%. At higher pressures, the discrepancy between the $\eta_{p,T}^{CH_4}$ data of Schley et al. and Evers et al. increases to as much as 2.5%, which greatly exceeds their combined uncertainty estimates.

The ratios $\eta_{0,T}^{H_2}/\eta_{0,T}^{He}$ and the viscosities $\eta_{0,T}^{H_2}$ and $\eta_{100,T}^{H_2}$ determined in this work are listed in Table VIII. Figure 5 compares our measurements of $\eta_{0,T}{}^{H_2}/\eta_{0,T}{}^{He}$ with other measurements and with a calculation using the H_2 correlation of Assael et al. [21] and the He–He

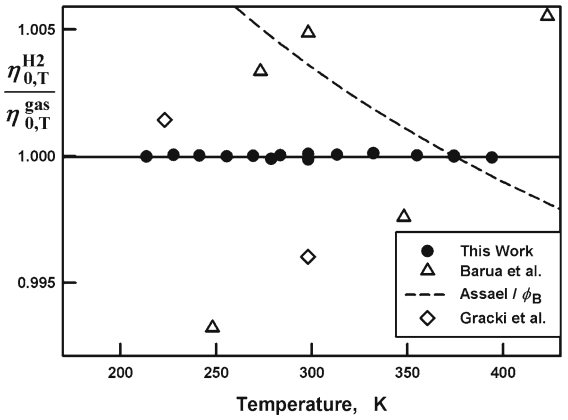

Fig. 5. Comparison of the ratio $\eta^{H_2}_{0,T}/\eta^{He}_{0,T}$ measured in this work with ratios computed from the data of Gracki et al. [24] and with a calculation that uses the correlation of Assael et al. [21] for H_2 and the He-He potential φ_B [11]. For the present measurements and the calculation, the baseline is Eq. (4) with the H_2 parameters in Table I. Barua et al. [30] measured CH_4 as well as H_2, so their data are presented as $\eta^{H_2}_{0,T}/\eta^{CH_4}_{0,T}$ divided by a baseline calculated from Eq. (4) and the parameters for H_2 and CH_4 in Table I.

potential φ_B [11]. Equation (4) with the parameters listed in Table I fits our H_2 data with an rms deviation of 0.007%. The uncertainty of our ratio data is 0.021%.

The curve in Fig. 5 combines values of $\eta^{H2}_{0,T}$ calculated from the correlation of Assael et al. [21] with values of $\eta^{He}_{0,T}$ calculated from the potential φ_B [11]. The uncertainty of the Assael et al. zero-density viscosity correlation is estimated to be $\pm 0.5\%$ in the temperature range from 200 to 360 K [21], which is an order of magnitude larger than the uncertainty of the *ab initio* value of $\eta^{He}_{0,T}$. This calculated ratio is consistent with our data within the uncertainties of the H_2 correlation between 270 and 400 K. At 214 K, the calculated ratio is 0.9% larger than our measured value.

Between 1963 and 1969, Flynn et al. used coiled capillary viscometers to measure absolute values of $\eta^{gas}_{p,T}$ for eight gases over a wide range of temperature and pressure [24, 30, 35]. Values of $\eta^{H_2}_{0,T}$ and $\eta^{He}_{0,T}$ extrapolated from the 223 and 298 K isotherms measured by Gracki et al. [24] were divided to give $\eta^{H_2}_{0,T}/\eta^{He}_{0,T}$ ratios. Figure 4 shows that these ratios differ from our data by less than 0.4%. Values of $\eta^{H_2}_{0,T}$ and $\eta^{CH_4}_{0,T}$ extrapolated from the isotherms measured by Barua et al. [30] were divided to

Table VIII. Viscosity of Hydrogen at Zero Density and 100 kPa

T (K)	$\eta_{0,T}^{H_2}/\eta_{0,T}^{He}$ ±0.024%	$\eta_{0,T}^{H_2}$ (μPa·s) ±0.084%	$\eta_{100,T}^{H_2}$(μPa·s) ±0.084%
213.615	0.44691	7.070	7.072
227.744	0.44746	7.391	7.393
241.269	0.44786	7.692	7.694
255.544	0.44822	8.004	8.005
269.369	0.44852	8.301	8.302
278.805	0.44864	8.500	8.501
283.570	0.44878	8.601	8.603
298.129	0.44902	8.905	8.906
298.142	0.44892	8.903	8.904
313.223	0.44919	9.214	9.215
332.201	0.44940	9.598	9.598
354.974	0.44954	10.048	10.049
374.388	0.44964	10.426	10.426
374.396	0.44962	10.426	10.426
394.209	0.44969	10.805	10.805

give $\eta_{0,T}^{H_2}/\eta_{0,T}^{CH_4}$ ratios. For a more direct comparison with our data, these latter ratios are shown in Fig. 5 relative to a *different* baseline calculated from Eq. (4) and the parameters for H_2 and CH_4 in Table I. Barua et al. [30] made fewer measurements at low densities than Gracki et al. [24] and the purity of their methane was only 99.4%. Thus, their $\eta_{0,T}^{H_2}/\eta_{0,T}^{CH_4}$ ratios are less reliable than those of Gracki et al. [24]. Nevertheless, at temperatures above 248 K, their ratios are consistent with our measurements to within 0.55%.

Figure 6 compares our measurements of the viscosity ratio $\eta_{0,T}^{Xe}/\eta_{0,T}^{He}$ with the measurements of Clarke and Smith [33] and with a calculation based on the potential of Dham et al. [8]. The baseline of Fig. 6 is Eq. (4) with the xenon parameters listed in Table I; the equation fits our data with an rms deviation of 0.059%. The uncertainty of our ratio data is 0.1%. Clarke and Smith's data deviate from ours by a maximum of 0.36% and above 220 K are within 0.15%.

The curve in Fig. 6 combines values of $\eta_{0,T}^{Xe}$ calculated from the potential of Dham et al., constructed largely with data measured at temperatures above 273 K [8], with values of $\eta_{0,T}^{He}$ calculated from the potential φ_B [11]. The calculated values are within 0.5% of our measured data at all temperatures.

We used calculated values of the Prandtl number in Eq. (3) to obtain the thermal conductivity $\lambda_{0,T}^{gas}$ for the monatomics argon and xenon. The

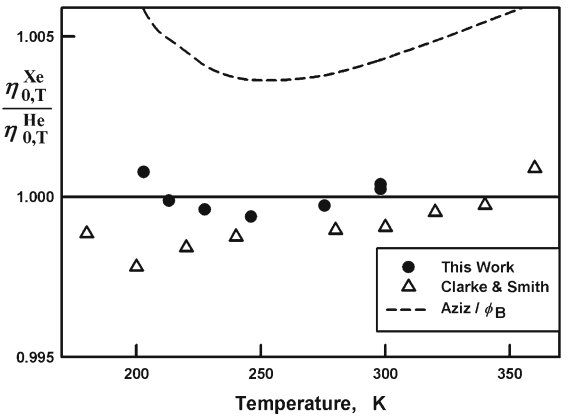

Fig. 6. Comparison of the ratio $\eta^{Xe}_{0,T}/\eta^{He}_{0,T}$ measured in this work with ratios measured by Clarke and Smith [33] and with a ratio determined using $\eta^{Xe}_{0,T}$ calculated from the Xe–Xe potential of Dham et al. [8] and $\eta^{He}_{0,T}$ calculated from the potential φ_B [10]. The baseline is Eq. (4) with the Xe parameters in Table I. (Clarke and Smith's ratio at 260 K is not shown due to an apparent typographical error for helium in Table II of Ref. 34.)

Prandtl number $Pr^{gas}_{0,T}$ is insensitive to the choice of pair potential used in the calculation, so it contributes a relative uncertainty to $\lambda^{gas}_{0,T}$ of only 0.00004 [1]. For argon we used the potential of Boyes [17], and for xenon we used the potential of Dham et al. [8] to determine $Pr^{gas}_{0,T}$.

Figure 7 shows ratios $\lambda^{Xe}_{0,T}/(\lambda^{Xe}_{0,T})_{Dham}$ where the denominator is the thermal conductivity of xenon calculated using the potential of Dham et al. [8], and the numerator is taken from one of three sources: this work, the correlation of Bich et al. [36], or the correlation used by NIST-23 [20]. The deviation between the correlation of Bich et al. and the values determined in this work is no more than 0.3%, which is within the correlation's stated uncertainty (0.3% at 298.15 K to 1% at 165 K) [36]. The deviation between the NIST-23 correlation and this work is no more than 1.3%, which is well within the correlation's estimated uncertainty of 6%.

The calculation of low-density transport properties using standard kinetic theory includes a contribution from bound pairs [7]. However, Curtiss [6] predicted that bound pairs make an additional contribution to low-density transport properties. At a reduced temperature of one, this additional contribution decreases the self-diffusion coefficient by 3.7% and the viscosity and thermal conductivity by 0.7%. The effects of bound pairs

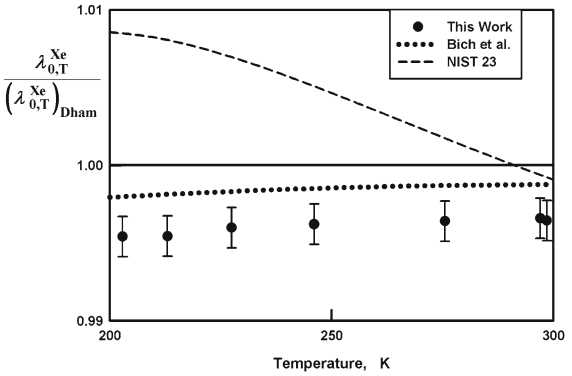

Fig. 7. Comparison of the ratios $\lambda_{0,T}^{Xe}/(\lambda_{0,T}^{Xe})_{Dham}$ determined in this work with the ratios derived from the correlations of Bich et al. [36] and of NIST-23 [20]. The denominator was calculated from the intermolecular potential of Ref. 8.

become significantly greater at lower temperatures. Curtiss quantified these effects in Table I of Ref. 6 by calculating collision integrals for a Lennard–Jones potential with and without the additional bound-pair contribution.

The potential of Dham et al. [8] was fit to measurements of the second virial coefficient [37] and viscosity [38]. Most of those measurements were taken above 273 K, where the additional bound-pair contribution for xenon is 0.3% or less, and the few data that were taken at lower temperatures were given a weight that was three times smaller [8]. Thus, the effect predicted by Curtiss would cause the viscosity measured at low temperatures to deviate below the viscosity $(\lambda_{0,T}^{Xe})_{Dham}$ predicted using the potential of Dham et al. and standard kinetic theory.

Figure 8 uses the ratio $\eta_{0,T}^{Xe}/(\eta_{0,T}^{Xe})_{Dham}$ to compare our data with Curtiss' prediction. As the temperature decreases, the ratio calculated from our data remains approximately constant, while the ratio calculated from Curtiss' prediction decreases; at our lowest temperature of 202 K, the discrepancy is 0.69%. Thus, the present data show no evidence of an additional bound-pair contribution to xenon's transport properties.

Also shown in Fig. 8 are the ratios $\eta_{0,T}^{Xe}/(\eta_{0,T}^{Xe})_{Dham}$ derived from the data of Clarke and Smith [33]; we converted their measured ratios $\eta_{0,T}^{Xe}/\eta_{0,T}^{He}$ to values of $\eta_{0,T}^{Xe}$ using the reference value $\eta_{0,298}^{He} = 19.833\,\mu$ Pa·s and the *ab initio* ratio $\left(\eta_{0,T}{}^{He}/\eta_{0,298}^{He}\right)_{ab\ initio}$. Although these ratios do

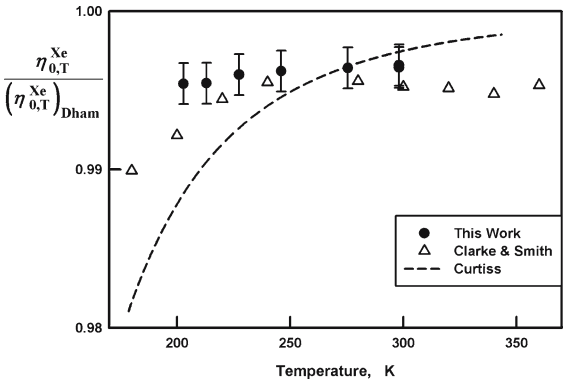

Fig. 8. Comparison of the ratios $\eta_{0,T}^{Xe}/(\eta_{0,T}^{Xe})_{Dham}$ determined in this work with the ratios derived from the data of Clarke and Smith [33] and with a ratio calculated using the additional bound pair contribution of Curtiss [6].

decrease with temperature, they do not decrease as rapidly as predicted by Curtiss. At the lowest temperature of 180 K, the discrepancy is 0.88%.

ACKNOWLEDGMENTS

The authors thank John Hurly for his thermophysical property calculations, Laurent Pitre for help with the design and construction of the flow control system, Roberto Gavioso for assistance with several measurements, John Wright for equipment loans and flow calibrations, and Greg Strouse and Dawn Cross for calibrating the thermometers. While at NIST, EFM was supported in part by an AAA/ANZ Education Fellowship.

REFERENCES

1. E. F. May, M. R. Moldover, R. F. Berg, and J. J. Hurly, *Metrologia* **43**:247 (2006).
2. M. R. Moldover, S. J. Boyes, C. W. Meyer, and A. R. H. Goodwin, *J. Res. NIST* **104**:11 (1999).
3. G. F. Strouse, D. R. Defibaugh, M. R. Moldover, and D. C. Ripple, in *Temperature: Its Measurement and Control in Science and Industry*, Vol. VII, *8th Int. Temp. Symp.*, D. C. Ripple, ed. (American Institute of Physics, New York, 2003), pp. 31–36.
4. M. R. Moldover, J. P. M. Trusler, T. J. Edwards, J. B. Mehl, and R. S. Davis, *J. Res. Natl. Bur. Stand.* (U.S.) **93**:85 (1988).
5. B. Fellmuth, J. Fischer, C. Gaiser, and W. Buck, BIPM Document CCT/05-02, http://www.bipm.fr/cc/CCT/Allowed/23/CCT_05_02.pdf (2005).
6. C. F. Curtiss, *J. Chem. Phys.* **97**:7679 (1992).

7. J. O. Hirschfelder, C. F. Curtiss, and R. B. Bird, *Molecular Theory of Gases and Liquids* (Wiley, New York, 1964).
8. A. K. Dham, W. J. Meath, A. R. Allnat, R. A. Aziz, and M. J. Slaman, *Chem. Phys.* **142**:173 (1990).
9. See, for example, R. Hellman, E. Bich, and E. Vogel, *Proc. 16th Symp. Thermophys. Props.*, Boulder, Colorado (July 31–August 4, 2006).
10. J. J. Hurly and M. R. Moldover, *J. Res. Natl. Inst. Stand. Technol.* (U.S.) **105**:667 (2000).
11. J. J. Hurly and M. R. Moldover, unpublished (2004); J. J. Hurly and J. B. Mehl, *J. Res. Natl. Inst. Stand. Technol.* **112**:75 (2007).
12. J. Kestin and W. Leidenfrost, *Physica* **25**:1033 (1959).
13. C. Evers, H. W. Lösch, and W. Wagner, *Int. J. Thermophys.* **23**:1411 (2002).
14. R. F. Berg, *Metrologia* **42**:11 (2005).
15. R. F. Berg, erratum to *Metrologia* **42**:11 (2005); *Metrologia* **43**:183 (2006).
16. R. F. Berg and S. A. Tison, *J. Res. Natl. Inst. Stand. Technol.* (U.S.) **109**:435 (2004).
17. S. J. Boyes, *Chem. Phys. Lett.* **221**:467 (1994).
18. J. J. Hurly, J. W. Schmidt, S. J. Boyes, and M. R. Moldover, *Int. J. Thermophys.* **18**:579 (1997).
19. E. Vogel, J. Wilhelm, C. Küchenmeister, and M. Jaeschke, *High Temp. High Press.* **32**:73 (2000).
20. E. W. Lemmon, M. O. McLinden, and M. L. Huber, *Reference Fluid Thermodynamic and Transport Properties*, NIST Standard Reference Database 23, Version 7.0, http://www.nist.gov/srd/nist23.htm (2002).
21. M. J. Assael, S. Mixafendi, and W. A. Wakeham, *J. Phys. Chem. Ref. Data* **15**:1315 (1986).
22. J. C. Rainwater and D. G. Friend, *Phys. Rev. A* **36**:4062 (1987).
23. E. W. Lemmon and R. T. Jacobsen, *Int. J. Thermophys.* **25**:21 (2004).
24. J. A. Gracki, G. P. Flynn, and J. Ross, *J. Chem. Phys.* **51**:3856 (1969).
25. J. Wilhelm and E. Vogel, *Int. J. Thermophys.* **21**:301 (2000).
26. E. Vogel, C. Küchenmeister, E. Bich, and A. Laesecke, *J. Phys. Chem. Ref. Data* **27**:947 (1998).
27. J. J. Hurly, K. A. Gillis, J. B. Mehl, and M. R. Moldover, *Int. J. Thermophys.* **24**:1441 (2003).
28. J. Kestin and J. Yata, *J. Chem. Phys.* **49**:4780 (1968).
29. P. Schley, M. Jaeschke, C. Küchenmeister, and E. Vogel, *Int. J. Thermophys.* **25**:1623 (2004).
30. A. K. Barua, M. Afzal, G. P. Flynn, and J. Ross, *J. Chem. Phys.* **41**:374 (1964).
31. S. Hendl and E. Vogel, *Fluid Phase Equilib*. **76**:259 (1994).
32. B. Najafi, Y. Ghayeb, J. C. Rainwater, S. Alavi, and R. F. Snider, *Physica A* **260**:31 (1998).
33. A. G. Clarke and E. B. Smith, *J. Chem. Phys.* **48**:3988 (1968)
34. A. G. Clarke and E. B. Smith, *J. Chem. Phys.* **51**:4156 (1969)
35. G. P. Flynn, R. V. Hanks, N. A. Lemaire, and J. Ross, *J. Chem. Phys.* **38**:154 (1963)
36. E. Bich, J. Millat, and E. Vogel, *J. Phys. Chem. Ref. Data* **19**:1289 (1990).
37. A. Michels, T. Wassenaar, and P. Louwerse, *Physica* **20**:99 (1954).
38. E. Vogel, *Ber. Bunsenges. Phys. Chem.* **88**:997 (1984).